GaAs/$Al_{0.8}Ga_{0.2}As$ avalanche photodiodes for soft X-ray spectroscopy

2014 JINST 9 P03014

(http://iopscience.iop.org/1748-0221/9/03/P03014)

PUBLISHED BY IOP PUBLISHING FOR SISSA MEDIALAB

RECEIVED: *December 10, 2013*
ACCEPTED: *February 10, 2014*
PUBLISHED: *March 25, 2014*

2014 JINST 9 P03014

GaAs/$Al_{0.8}Ga_{0.2}As$ avalanche photodiodes for soft X-ray spectroscopy

R.B. Gomes, C.H. Tan, X. Meng, J.P.R. David and J.S. Ng[1]

Department of Electronic & Electrical Engineering, University of Sheffield, Mappin Street, Sheffield, S1 3JD, U.K.

E-mail: j.s.ng@sheffield.ac.uk

ABSTRACT: The soft X-ray spectroscopic performance of a GaAs/$Al_{0.8}Ga_{0.2}As$ Separate Absorption and Multiplication (SAM) APD was assessed at room temperature using a ^{55}Fe source. An energy resolution of 1.08 keV (FWHM) was achieved for the 5.9 keV X-rays, at an avalanche gain of 3.5. The avalanche gain also improved the minimum detectable energy from 4.8 keV at unity gain to about 1.5 keV at a gain of 5. Through avalanche statistics analyses, we confirmed that (i) the APD's FWHM was degraded by X-ray photon absorption within the avalanche region, and (ii) photon absorption in/near the n-cladding layer contributed to an undesirable secondary peak in the spectrum.

KEYWORDS: X-ray detectors; Detector modelling and simulations II (electric fields, charge transport, multiplication and induction, pulse formation, electron emission, etc)

[1]Corresponding author.

doi:10.1088/1748-0221/9/03/P03014

Contents

2014 JINST 9 P03014

1 Introduction

X-ray detectors for harsh thermal environments require the detectors to operate without cryogenic cooling for higher stability and lower operational cost. Many wide band gap compound semiconductors have been investigated for room (and higher) temperature operation. Comprehensive reviews on such materials can be found in refs. [1, 2]. Some of the best results have been achieved with GaAs and SiC coupled with ultra-low noise electronics. For example, Bertuccio et al. have reported SiC X-ray detectors with sub-keV energy resolution operating in a wide temperature range [3]. Most of the reported III-V X-ray detectors are however based on GaAs, which has mature wafer growth technology. Its material properties are advantageous in that GaAs offers more efficient absorption than Si, while offering lower leakage currents than Ge, whose energy gap is much narrower. Several research groups have also demonstrated GaAs detector arrays for X-ray photons [4–6].

When using detectors for soft X-ray photons, the number of electron-hole-pairs and hence the magnitude of photocurrent generated by each absorbed photon is small than when detecting hard X-ray photons. It is thus attractive to have very low noise amplification of this electrical current, achieved using either low noise internal gain in the detector or ultra low noise pre-amplifiers. The former can be achieved by using well-designed avalanche photodiodes (APDs). APDs provide avalanche gain, M, via the impact ionization process, in which an energetic electron (or a hole) gives up its energy to create another electron and a hole. Due to statistical variation in the impact ionization process, the avalanche gain does bring added noise, which is usually characterized by the excess noise factor. Design of an APD can greatly influence the level of the added noise, and in many applications, using a well-designed APD improves the overall signal-to-noise ratio, compared to using a photodiode that does not provide gain.

For X-ray photon detection, APDs can offer improvement in signal-to-noise ratio, without degrading spectral resolution. Theoretical work has shown that, statistical variation in the avalanche

Table 1. Details of the GaAs/$Al_{0.8}Ga_{0.2}As$ SAM APD wafer.

250 nm p^+ GaAs (cladding)
430 nm i – GaAs (absorption layer)
50 nm p – GaAs (field-control layer)
80 nm p - $Al_{0.8}Ga_{0.2}As$ (field-control layer)
220 nm i - $Al_{0.8}Ga_{0.2}As$ (avalanche layer)
100 nm n^+ $Al_{0.8}Ga_{0.2}As$ (cladding)
200 nm n^+ GaAs (buffer)
n^+ GaAs substrate

gain process reduces rapidly as the number of carriers generated by X-ray photon absorption increase [7, 8]. Also, to maintain spectral resolution, X-ray photons should be predominantly absorbed in a non-avalanche region in the APD [7], which favours the configuration of SAM APDs.

A GaAs-based SAM APDs is therefore an attractive option for X-ray APDs. In fact a GaAs-based SAM APD [9] was reported for X-ray detection, with energy resolutions of 1.95 keV and 0.9 keV achieved at gains of unity and 4.1 respectively, for 13.9 keV X-rays. However, due to understanding of impact ionization then, a complicated GaAs/AlGaAs multiple-quantum wells design for the avalanche region was used. With improved impact ionization knowledge [10] and the recent understanding that X-ray APD is not affected significantly by fluctuation in the avalanche gain process, a much simpler design can be used for GaAs-based SAM APD, without compromising its performance. More specifically a layer of $Al_{0.8}Ga_{0.2}As$, whose energy bandgap is 2.1 eV, can suffice as the avalanche region. The simplification of the APD design is not trivial, as a simple APD design often means greater tolerance in the wafer growth and hence better uniformity across a given wafer and better yield from repeated wafer growth runs. It may not be a coincidence that the APD in ref. [10] did not achieve full-depletion as intended.

In this work, we report a GaAs/$Al_{0.8}Ga_{0.2}As$ SAM APD and its characterization data for soft X-ray detection at room temperature. The effects of avalanche gain on the energy resolution of the detected X-ray peak and the minimum detectable energy (MDE) were experimentally obtained. The data was also analyzed using the avalanche statistics model presented in [7].

2 Wafer details and Capacitance-Voltage characteristics

Details of the GaAs/$Al_{0.8}Ga_{0.2}As$ SAM APD wafer grown on an n^+ GaAs substrate by Molecular Beam Epitaxy (MBE) is shown in table 1. It had a 0.43 μm thick GaAs absorption layer and a 0.22 μm thick $Al_{0.8}Ga_{0.2}As$ avalanche layer. The p^+ and n^+ cladding layers of the diode were doped with Be and Si respectively to $\sim 2\times10^{18}$ cm^{-3}. A p-type (Be doped) layer made up of GaAs and $Al_{0.8}Ga_{0.2}As$ separated the absorption and the avalanche layers to ensure low and high electric fields in the two layers, respectively. A fully-depleted GaAs absorption layer will have efficient collection of photogenerated carriers without providing unwanted avalanche multiplication.

2014 JINST 9 P03014

The absorption region used GaAs, instead of $Al_{0.8}Ga_{0.2}As$, so that future APD design can have much thicker absorption regions without lattice-mismatch problems. The current design compromised on absorption efficiency caused by the too-thin absorption layer, in order to ensure a fully-depleted APD at this early stage of device development.

The wide bandgap $Al_{0.8}Ga_{0.2}As$ was used in the avalanche region for its high temperature performance [11]. The $Al_{0.8}Ga_{0.2}As$ avalanche region was kept thin in order to (i) minimize undesirable X-ray photon absorption in the multiplication region [7], and (ii) minimize presence of defects caused by the slight-mismatch between $Al_{0.8}Ga_{0.2}As$ and GaAs.

Circular mesa diodes of diameters ranging from 50 to 400 μm were fabricated from the wafer by using standard photolithography. Au/Zn/Au annular contacts were deposited on the top p^+ layer of the diode to form ohmic p^+ contacts. The ohmic n^+ contacts were formed by using In/Ge/Au. The mesa diodes were created by wet chemical etching using a solution of hydrobromic acid, acetic acid, and potassium dichromate (ratio of 1:1:1).

In order to assess the thickness of key layers within the wafer, Capacitance-Voltage (C-V) measurements were carried out on different-sized APDs. The capacitance of the APD scaled with junction area, as expected. C-V data of a 200 μm diameter APD is shown in figure 1. The sudden decrease in capacitance at $\sim$ 10 V indicated a punch-through voltage (the minimum voltage required to fully deplete the APD) of $\sim$ 10 V. Analysing the C-V data with an electrostatic model, the thickness of the undoped absorption and avalanche regions were estimated to be 0.43 and 0.22 μm respectively. The fitting from the electrostatic model analysis is also shown in figure 1. For reverse bias $<$ 10 V, the depletion region did not include the i-$Al_{0.8}Ga_{0.2}As$ avalanche region, allowing us to estimate the i-GaAs absorption layer thickness accurately. With that information, it was then possible to estimate the i-$Al_{0.8}Ga_{0.2}As$ avalanche region thickness using capacitance values at reverse bias $>$ 10 V. Information deduced from the C-V analysis were later used in modelling the APD's X-ray response.

3 X-ray response

3.1 Pulse height spectra

To facilitate X-ray measurements, the 200 μm diameter APDs were packaged into TO-5 headers using a gold wire bonder. A TO-5 header containing the APDs was mounted on a copper holder, which was housed in a metal dewar. Prior to X-ray response measurements, dark reverse current-voltage (I-V) characteristics of the APD under test was measured. Typical I-V data of the APDs are shown in figure 2. The dark current increased rapidly with voltage for voltage beyond 21 V due to significant avalanche gain, which eventually led to a sharp breakdown at 22 V. Prior to avalanche breakdown, the dark current was dominated by surface-related mechanism.

For the X-ray response measurement, a 185 MBq ^{55}Fe radioisotope source with characteristic Mn K_α and K_β peaks at 5.9 and 6.49 keV respectively was irradiated on the APD placed 0.5 cm away. The APD was reverse-biased using a Keithley 2400 SMU through a charge sensitive preamplifier (Amptek A250CF). The signal from the preamplifier was shaped using a semi-Gaussian shaping amplifier (Ortec 570), with an optimum shaping time of 2 μs. The amplified pulse was then digitised and fed to a multichannel analyser (MCA) interfaced with a computer to yield pulse height spectra. Spectra were collected for a number of reverse bias voltages at room temperature.

2014 JINST 9 P03014

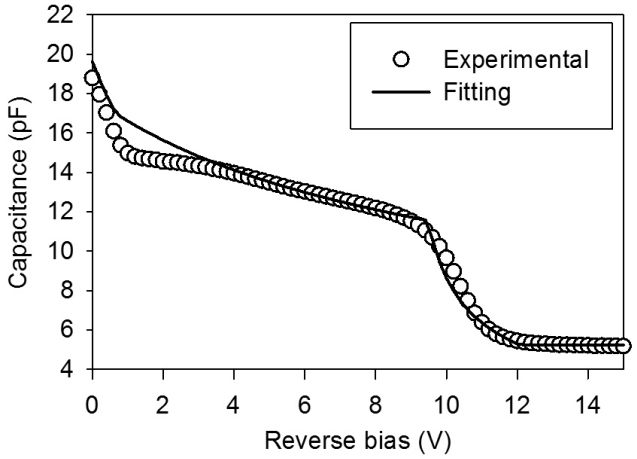

Figure 1. C-V data (line) and fitting from electrostatic model (symbols) for a 200 μm diameter APD. The APD was fully depleted by $\sim$ 10 V.

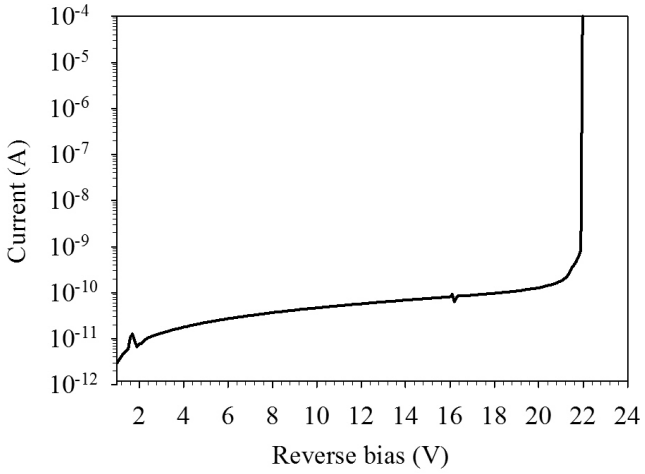

Figure 2. Leakage current versus reverse bias data of the APD (200 μm diameter).

Pulse height spectra obtained from the APD irradiated with the ^{55}Fe isotope, with reverse bias voltage ranging from 9.97 to 21.53 V, are shown in figure 3. The 5.9 keV X-ray peak moved away from the electronic noise floor as the reverse bias voltage and hence avalanche gain increased, thus improving the signal-to-noise ratio of the measurement system. The maximum useful gain before breakdown depends on the device leakage current, which adds noise to the measurements. The bias resistor used was large (330 MΩ), in order to reduce the thermal noise in the system. At higher bias, the device leakage current was significant, resulting in appreciable voltage drops across the bias resistor, hence the applied voltage values were appropriately corrected to account for this. As the reverse bias increased, a distinct secondary peak at lower channel numbers can be observed. Its origin will be discussed in section 4. Since most of the carriers collected as signals were created by photons absorption in layers above or within the p^+ $Al_{0.8}Ga_{0.2}As$ layer, pure injection of electrons predominantly accounted for the main detected peak.

2014 JINST 9 P03014

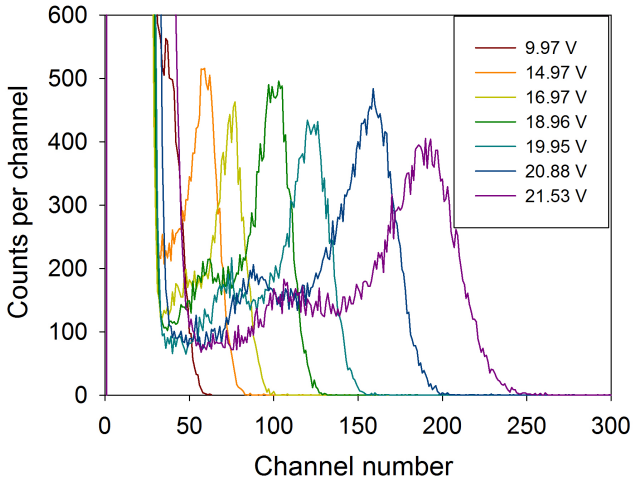

Figure 3. Pulse height spectra obtained from the APD irradiated with a ^{55}Fe source, as a function of reverse bias voltage.

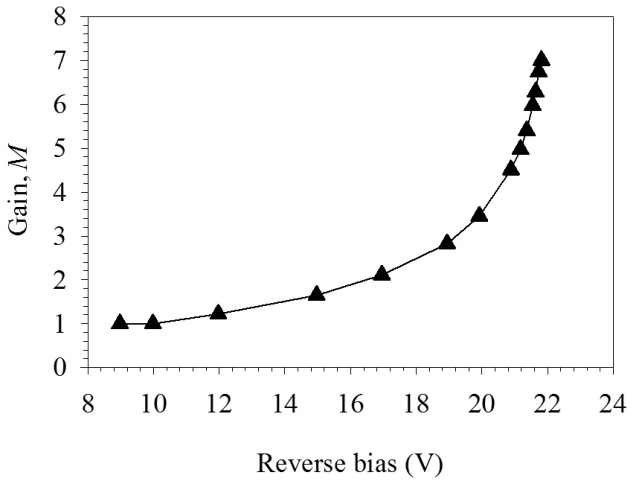

Figure 4. Approximate avalanche gain values deduced from X-ray measurements on the APD (line is for visualization purposes).

Approximate values of M were given by the ratio of the peak channel number (from Gaussian peak fitting) for each bias to the peak channel number at 9 V (deemed to have $M = 1$, due to absence of change in peak channel number between 9 and 10 V and separate photocurrent measurements carried out on this wafer). The MCA was also calibrated with zero-offset such that channel number zero represents the actual zero of the detection system. Figure 4 shows the approximate mean gain values obtained.

3.2 Energy resolution

In order to analyse energy resolution of the APDs, resolution due to the measurement setup itself was measured in electronic noise tests. Pulses from a pulse generator were fed to the test signal input of the preamplifier, whilst the preamplifier was still connected to the device-under-test. Hence the electronic noise measured includes the noise due to the device's leakage current and

2014 JINST 9 P03014

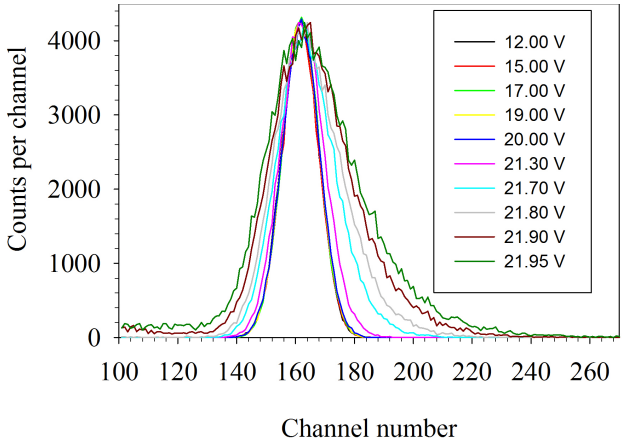

Figure 5. Spectra from electronic noise tests performed on the APD at different reverse biases.

capacitance, the preamplifier, the post amplifier, and stray capacitances between the device and the preamplifier input. The resultant noise spectra for the APD at different reverse biases are compared in figure 5. The spectra became broader and less symmetrical as the reverse bias increases, which was attributed to increase in leakage current.

For the raw X-ray spectra, the channel number information was converted into energy, using the 0 eV peak (noise peak) and the detected X-ray peak as references. FWHM of the 5.9 keV X-ray peak was then obtained by fitting Gaussian curves to the peak. Figure 6 plots the APD's FWHM values with those from electronic noise tests as functions of reverse bias voltage. Also, the FWHM values from electronic noise tests were smaller than those from the X-ray spectra. As reverse bias and hence avalanche gain increased, the X-ray spectra FWHM decreased initially, before increasing again. This trend was consistent with observations from ref. [9]. The best FWHM from the 5.9 keV X-ray detection was ~ 1.1 keV at 20.0 V.

Another important parameter for detection in this range is the minimum detectable energy (MDE) of the APD, which is defined as the energy at which the 0 keV and 5.9 keV peaks in the pulse height spectra intersect, for this work. For cases where the two peaks do not intersect, the MDE was taken as the lowest energy that registers < 1 count. Data of MDE versus reverse bias are plotted in figure 7. The MDE reduced rapidly from ~ 5 keV at 12 V to ~ 1.5 keV at 21.5 V. When the applied reverse bias was greater than 21.5 V, the APD approaches breakdown and large dark current degraded the MDE due to the growing noise peak in the pulse height spectra.

4 Discussion

The fano-limited energy resolution for the energy peak is given by $\Delta E_F = 2.35(fE\varepsilon)^{1/2}$ [12], where f is the fano factor, E is the incident photon energy and ε is the pair creation energy. Using $f = 0.12$ and $\varepsilon = 4.18$ eV for GaAs [13], $\Delta E_F = 129$ eV at 5.9 keV is predicted for GaAs. This is significantly smaller than our best experimental FWHM values from X-ray detection (1.08 keV at $M = 3.5$) and the electronic noise tests (800 eV at non-unity gains), which is not surprising considering the relatively large detector's capacitance (~ 5 pF). While it is clear that reducing the APD's capacitance and the amplifier's noise will improve the experimental FWHM for the APD, the secondary peaks in the X-ray spectra (figure 3) do broaden the main peak at 5.9 keV.

2014 JINST 9 P03014

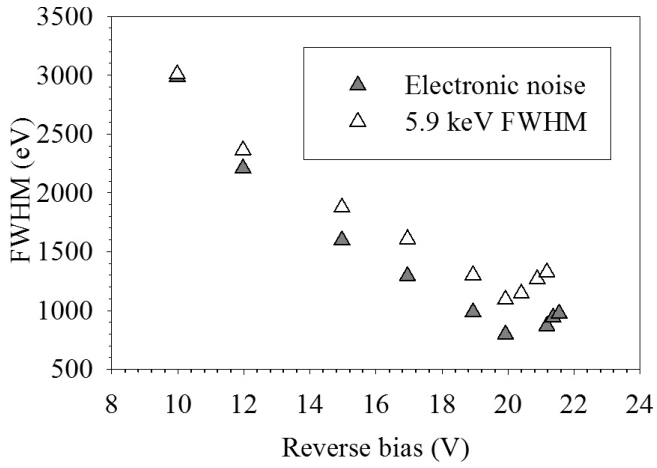

Figure 6. FWHM values obtained from ^{55}Fe isotope irradiated on the APD are compared to FWHM values from the electronic noise tests.

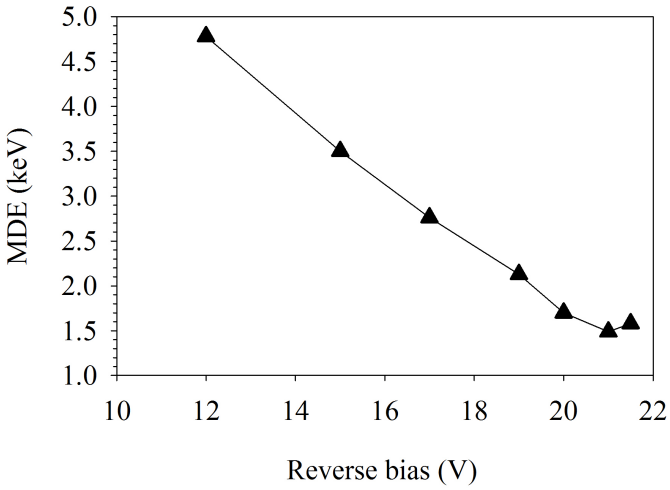

Figure 7. Variation of the low energy threshold with increasing reverse bias.

In our attempt to determine the origin(s) of the secondary peaks in the X-ray spectra, avalanche gain statistics were simulated for the detector using the Random Path Length (RPL) model for X-ray APD [7]. The simulations took into account the relative intensities of the $K\alpha$ and $K\beta$ X-rays from the ^{55}Fe source, assuming an emission probability ratio of $P_{K\beta}/P_{K\alpha} = 0.138$ [14]. Appropriate linear absorption coefficients, γ (given by mass absorption coefficient multiplied by the material's density), were assigned to the GaAs and AlGaAs layers to accurately describe X-ray photon absorption profile within the detector [15]. The number of electron-hole pairs (ehps) produced by an absorbed X-ray photon was given by (E/ε), with the material-specific value for ε. All ehps were assumed to be created at the point of interaction (a reasonable assumption for low energy X-rays where the mean free path length of the photon is still smaller than the total detector thickness). For simplicity, complete charge collection was assumed for ehps created within and above the n^+ $Al_{0.8}Ga_{0.2}As$ layer, although low energy tails in the experimental results do suggest incomplete charge collection.

2014 JINST 9 P03014

Table 2. Values of parameters used in avalanche gain statistics simulation of the APD.

	ε (eV)	γ @ 5.9 keV (cm^{-1}) [15]	γ @ 6.49 keV (cm^{-1}) [15]	Impact ionization coefficients (cm^{-1}) [16]
GaAs	4.21	833.7	640.5	Zero
$Al_{0.8}Ga_{0.2}As$	5.25	638.8	490.9	$\alpha(\xi) = 3.18 \times 10^5 \exp\left[\left(1.04 \times 10^6/\xi\right)^{1.67}\right]$ $\beta(\xi) = 3.55 \times 10^5 \exp\left[\left(1.12 \times 10^6/\xi\right)^{1.85}\right]$

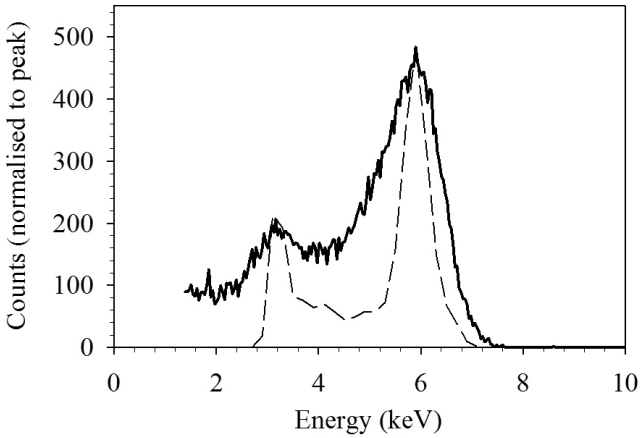

Figure 8. Comparison of simulated gain spectrum (dashed line) and experimental spectrum (solid line) for the APD at M = 4.5.

The avalanche gain experienced by each carrier (electron and hole) was then calculated using the RPL model. The model assumed the electric field dependences of electron and hole impact ionisation coefficients, $\alpha(\xi)$ and $\beta(\xi)$, from [16] for $Al_{0.8}Ga_{0.2}As$. Impact ionization threshold energy of 2.23 eV was also taken from [16] to account for the 'dead space' in impact ionization [17]. The counts of the simulated spectrum were normalised to those of the experimental spectra for ease of comparison. Values for ε, γ, $\alpha(\xi)$, and $\beta(\xi)$ of GaAs and $Al_{0.8}Ga_{0.2}As$ used in the simulations are given in table 2.

The simulated gain spectrum is compared to the measured spectrum for the APD at $M = 4.5$ in figure 8, which show agreement in terms of the positions and relative heights of the main and the secondary peaks. Through simulations, we confirm that the appearance of secondary peak is due to the difference in avalanche gains experienced by the ehps created in/near the n^+ $Al_{0.8}Ga_{0.2}As$ layer and those created in the layers above it. The former, which relies on holes to undergo impact ionization will experience a lower avalanche gain than the latter, because $\beta < \alpha$ in $Al_{0.8}Ga_{0.2}As$. This will produce smaller detector's signals, resulting in an additional peak at lower energy. As the thickness of the n^+ $Al_{0.8}Ga_{0.2}As$ layer is much thinner than the combined thickness of all layers above it, there are far fewer ehps created in the n^+ $Al_{0.8}Ga_{0.2}As$ layer than in the layers above, so the additional peak is smaller in magnitude compared to the main peak. The overall outcome is that a smaller undesirable peak appears at energies lower than the 5.9 keV peak. Similarly, photon absorption within the avalanche layer results in counts with channels between the main and the secondary peaks.

2014 JINST 9 P03014

The relative height of the secondary peak can be reduced by increasing the thickness of the undoped GaAs layer, which is also required for increasing detection efficiency and decreasing the detector's capacitance. A reasonable thickness for the GaAs absorption layer is $\sim 10\,\mu$m, the attenuation length for 5.9 keV photons.

5 Conclusions

GaAs/ $Al_{0.8}Ga_{0.2}As$ SAM APDs were demonstrated as room temperature detector soft X-ray photons. The avalanche gains from the APDs improve the energy resolution and MDE. The best energy resolution of 1.08 eV (FWHM) for the 5.9 keV line was achieved at a gain of 3.5. An APD design with a much thicker GaAs absorber region would improve the APD's performance by reducing the capacitance, increasing the quantum efficiency (particularly at higher energies), and reducing the prominence of the unwanted secondary peak at low channel numbers.

Acknowledgments

The work was funded by U.K. Science and Technology Facilities Council (ST/H000127/1). R.B. Gomes would also like to acknowledge the University of Sheffield for the PhD scholarship. J.S. Ng would like to acknowledge the Royal Society for her University Research Fellowship.

References

[1] D.S. McGregor and H. Hermon, *Room-temperature compound semiconductor radiation detectors*, *Nucl. Instrum. Meth.* **A 395** (1997) 101.

[2] P.J. Sellin, *Recent advances in compound semiconductor radiation detectors*, *Nucl. Instrum. Meth.* **A 513** (2003) 332.

[3] G. Bertuccio, R. Casiraghi, A. Cetronio, C. Lanzieri and F. Nava, *Silicon carbide for high resolution X-ray detectors operating up to 100°C*, *Nucl. Instrum. Meth.* **A 552** (2004) 413.

[4] G. Bertuccio, A. Pullia, J. Lauter, A. Forster and H. Luth, *Pixel X-ray detectors in epitaxial gallium arsenide with high-energy resolution capabilities (Fano factor experimental determination)*, *IEEE Trans. Nucl. Sci.* **44** (1997) 1.

[5] G.C. Sun et al., *X-ray detector with thick epitaxial GaAs grown by chemical reaction*, *IEEE Trans. Nucl. Sci.* **50** (2003) 1036.

[6] G.I. Ayzenshtat et al., *X-ray and γ-ray detectors based on GaAs epitaxial structures*, *Nucl. Instrum. Meth.* **A 531** (2004) 97.

[7] C.H. Tan et al., *Avalanche Gain and Energy Resolution of Semiconductor X-ray Detectors*, *IEEE Trans. Electron Dev.* **58** (2011) 1696.

[8] R.J. McIntyre, *The distribution of gains in uniformly multiplying avalanche photodiodes: Theory*, *IEEE Trans. Electron Dev.* **19** (1972) 703.

[9] J. Lauter, D. Protic, A. Forster and H. Luth, *AlGaAs/GaAs SAM-avalanche photodiode: An X-ray detector for low energy photons*, *Nucl. Instrum. Meth.***A 356** (1995) 324.

[10] C.K. Chia et al., *Multiplication and excess noise in $Al_xGa_{1-x}As$/GaAs multilayer avalanche photodiodes*, *J. Appl. Phys.* **94** (2003) 2631.

2014 JINST 9 P03014

[11] J.E. Lees et al., *Development of high temperature AlGaAs soft X-ray photon counting detectors*, 2011 *JINST* **6** C12007.

[12] G.F. Knoll, *Radiation detection and measurement*, John Wiley & Sons Inc., New York, U.S.A. (2000).

[13] G. Bertuccio and D. Maiocchi, *Electron-hole pair generation energy in gallium arsenide by x and gamma photons*, *J. Appl. Phys.* **92** (2002) 1248.

[14] U. Schötzig, *Half-life and X-ray emission probabilities of* ^{55}Fe, *Appl. Radiat. Isot.* **53** (2000) 469.

[15] J.H. Hubbell and S.M. Seltzer, *Tables of x-ray mass attenuation coefficients and mass energy-absorption coefficients 1 keV to 20 MeV for elements Z = 1 to 92 and 4 additional substances of dosimetric interest*, http://www.nist.gov/pml/data/xraycoef/index.cfm.

[16] B.K. Ng et al., *Avalanche multiplication characteristics of* $Al_{0.8}Ga_{0.2}As$ *diodes*,*IEEE Trans. Electron Dev.* **48** (2001) 2198.

[17] R.B. Gomes, C.H. Tan, J.E. Lees, J.P.R. David and J.S. Ng, *Effects of Dead Space on Avalanche Gain Distribution of X-Ray Avalanche Photodiodes*, *IEEE Trans. Electron Dev.* **59** (2012) 1063.

2014 JINST 9 P03014